Naval Research Laboratory
Washington, DC 20375-5320

NRL/MR/6790--98-8125

Precision-Scale Explosion Experiments Using Laser-Driven Shocks

J. Grun
R. Burris
A. Fisher
J. Huba
G. Joyce
S. Slinker

Beam Physics Branch
Plasma Physics Division

J. R. Barthel
J. W. Wiehe

Maxwell Laboratories, Inc. La Jolla, CA

J. Crawford

Southwest Texas State University, San Marcos, TX

K. Evans

Sachs Freeman Associates, Landover, MD

I. Kohlberg

Kohlberg Associates Inc., Alexandria, VA

C. K. Manka
J. Resnick

Research Support Instruments, Lanham, MD

B. H. Ripin

American Physical Society, College Park, MD

March 13, 1998

REPORT DOCUMENTATION PAGE

Form Approved
OMB No. 0704-0188

1. AGENCY USE ONLY (*Leave Blank*)	2. REPORT DATE	3. REPORT TYPE AND DATES COVERED
	March 13, 1998	Interim Report

4. TITLE AND SUBTITLE

Precision-Scale Explosion Experiments Using Laser-Driven Shocks

5. FUNDING NUMBERS

6. AUTHOR(S)

J. Grun, J.R. Barthel,[1] R. Burris, J. Crawford,[2] K. Evans,[3] A. Fisher, J. Huba, G. Joyce, I. Kohlberg,[4] C.K. Manka,[5] J. Resnick,[5] R.H. Ripin,[6] S. Slinker, and J.W. Wiehe[1]

7. PERFORMING ORGANIZATION NAME(S) AND ADDRESS(ES)

Naval Research Laboratory
Washington, DC 20375-5320

8. PERFORMING ORGANIZATION REPORT NUMBER

NRL/MR/6190--98-8125

9. SPONSORING/MONITORING AGENCY NAME(S) AND ADDRESS(ES)

Defense Special Weapons Agency
Alexandria, VA 22310

10. SPONSORING/MONITORING AGENCY REPORT NUMBER

11. SUPPLEMENTARY NOTES

[1]Maxwell Laboratories, Inc., La Jolla, CA 92038
[2]Southwest Texas State University, San Marcos, TX 78666
[3]Sachs Freeman Associates, Landover, MD 20785
[4]Kohlberg Associates Inc., Alexandria, VA 22304
[5]RSI, Lanham, MD 20706
[6]APS, College Park, MD 20740

12a. DISTRIBUTION/AVAILABILITY STATEMENT

Approved for public release; distribution unlimited.

12b. DISTRIBUTION CODE

13. ABSTRACT (*Maximum 200 words*)

The Naval Research Laboratory uses shock initiated by a powerful laser pulse to perform precision-scale measurements of hydrodynamic phenomena relevant to nuclear and conventional explosions, and to supernovae. A pulse from NRL's 1.5-kJ Pharos III laser is focused onto the surface of a period-sized piece of material placed in ambient gas. The laser heats the material to a few hundred eV creating a miniature explosion which launches a shock with multi-kilobar pressures and material flows with Mach number of a few hundred. This method has been used to perform the first measurements on a shock instability in a uniform ambient, the first measurements of shock decursors, and detailed measurements of shock precursors.

14. SUBJECT TERMS

Precision-scale
Shocks
Explosion

15. NUMBER OF PAGES

15

16. PRICE CODE

17. SECURITY CLASSIFICATION OF REPORT	18. SECURITY CLASSIFICATION OF THIS PAGE	19. SECURITY CLASSIFICATION OF ABSTRACT	20. LIMITATION OF ABSTRACT
UNCLASSIFIED	UNCLASSIFIED	UNCLASSIFIED	UL

NSN 7540-01-280-5500

Standard Form 298 (Rev. 2-89)
Prescribed by ANSI Std 239-18
298-102

CONTENTS

Precision-Scale Explosion Experiments Using Laser-Driven Shocks

J. Grun,[1] J.R. Barthel,[2] R. Burris,[1] J. Crawford,[3] K. Evans,[4] A. Fisher,[1] J. Huba,[1] G. Joyce,[1] I. Kohlberg,[5] C.K. Manka,[6] J. Resnick,[6] B.H. Ripin,[7] S. Slinker,[1] and J.W. Wiehe[2]

[1] Plasma Physics Division, Naval Research Laboratory, Washington DC 20375
[2] Maxwell Laboratories, Inc., La Jolla, CA 92038
[3] Physics Dept., SouthWest Texas State University, San Marcos TX 78666
[4] Sachs Freeman Associates, Landover, MD 20785
[5] Kohlberg Associates Inc., Alexandria, VA 22304
[6] Research Support Instruments, Lanham, MD. 20706
[7] American Physical Society, College Park, MD 20740

The Naval Research Laboratory uses shocks initiated by a powerful laser pulse to perform precision-scale measurements of hydrodynamic phenomena relevant to nuclear and conventional explosions, and to supernovae. A pulse from NRL's 1.5-kJ Pharos III laser is focused onto the surface of a period-sized piece of material placed in ambient gas. The laser heats the material to a few hundred eV creating a miniature explosion which launches a shock with multi-kilobar pressures and material flows with Mach numbers of a few hundred. This method has been used to perform the first measurements on a shock instability in a uniform ambient, the first measurements of shock decursors, and detailed measurements of shock precursors.

Introduction

A laser pulse can be focused with high intensity onto a piece of material placed in an ambient atmosphere, ablating the material and, thereby, producing a Taylor-Brode-Sedov shock not unlike shocks generated by more conventional means such as chemical explosions or shock tubes (Figure 1). [1] Laser-generated shocks have characteristics that make them well suited for precision-scale simulations of phenomena that were traditionally studied using nuclear tests or explosives. The overpressures achievable with laser generated shocks are very high and are much higher than overpressures achievable with chemical explosives. To illustrate this Figure 2 plots the overpressures of a laser-generated shock as a function of distance from the explosion scaled using the Sachs scaling law. [2] This law, which is based on geometrical similarity principles and conservation of momentum, is used to compare experiments performed with different explosive yields and different ambient pressures. Also plotted are curves expected of an ideal shock and a shock created with chemical and nuclear explosives. This figure shows that laser-produced shocks follow the ideal scaling law to much higher pressures than shocks produced with chemical explosives: Pressure greater than 100kbar is produced in air with lasers (at easily diagnosable distances), which is more than 1000 times greater than pressure from conventional explosives. In addition, the 'explosion' of laser-heated material has a very high energy to mass ratio (typically Gjoule/gm) so that the shock produced is more like a nuclear or an ideal shock than a shock produced by a chemical explosion. Moreover, since

Manuscript approved January 12, 1998.

a laser-explosion has little mass (typically μgm), the shock can be observed for a long time without being overrun by explosion products. This is especially advantageous when shocks reflecting back towards the source of the explosion need to be studied or measurements need to be taken over long periods of time. Finally, laser-shocks are produced on a small scale (typically cm) in a laboratory setting, so that precise measurements, shot repetition for statistics, and variation of parameters are much easier to do than is the case with traditional field experiments.

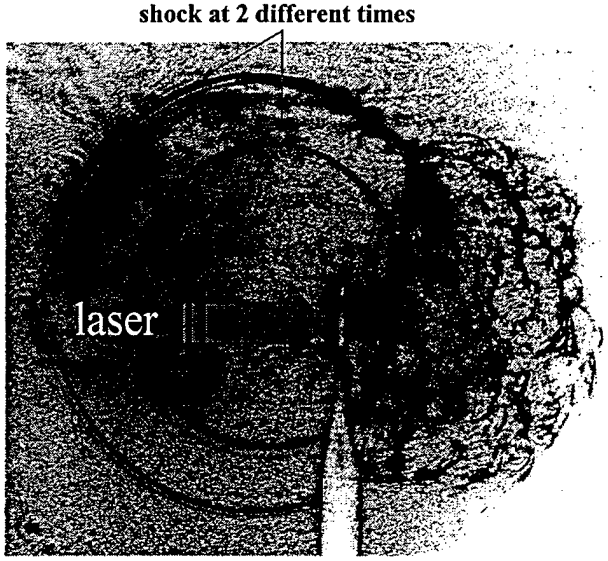

Figure 1

A laser focused on a small piece of material can create powerful shocks and high Mach number turbulence. By appropriate choice of target experiments can be designed to produce shocks without turbulence. This figure is a dark-field photograph taken at two instances in time on the same piece of film. This accounts for the double shock.

On the negative side, typical laser-produced shocks are thin (<mm). Because of this impulses are low so that it is difficult to have the shocks move or bend substantial (say ~ mm) thickness of material. Moreover, typical shock-material interaction time scales are nanoseconds to microseconds and for such short durations the time dependence of material stress must be carefully considered. Thus, experiments involving the coupling of hydrodynamics to structures are difficult to perform in this manner.

In our laboratory we have used the laser-shock technique to study phenomena such as crater formation and shock coupling to solids, [3] amplification of turbulence by high mach number shocks, [4] multi-burst explosions, [5] high and low altitude nuclear explosion effects, [6, 7] and shock instabilities [8]. In this article we will summarize a few examples of our work. We will begin by discussing the first measurements of an instability in adiabatic shocks propagating through a uniform, highly compressible medium. [8] The common wisdom, heretofore, was that shocks in a uniform ambient are stable. [9] The shock instability we measured may occur in supernovae and could explain why optical images of middle-aged an older supernovae appear filamentary. The same instability in swept up shells of interstellar gas may provide the initial conditions for gravitational collapse leading to the formation of stars and to the formation of globular clusters. [9] This study is a good example of the scalability of our small-scale laboratory experiment even to phenomena occurring on astronomical temporal and spatial scales. The second example will describe the first measurements of a shock-decursor, a phenomenon which occurs when a shock passes over a certain type of a non-ideal surface. [Grun, et al., 1991 in ref 7] Subsequent to our experiment the decursor was observed and measured on a much larger scale underground nuclear test called Diamond Fortune.[13] We end by describing a recent experiment which studied a precursor shock propagating over a hot thermal layer. [Grun, et al., 1997 in ref. 7] This experiment was successfully simulated with a code previously validated using large-scale

high-explosive tests with 12 orders of magnitude higher energies: Measured and simulated parameters agreed to ~ 10%. The code was not altered to simulate our experiment nor did it have any free parameters that could be adjusted to force a better fit. Together, these examples demonstrate that precision-scale laser-laboratory experiments can often be good surrogates for infrequent, expensive, and hard to diagnose large-scale tests, can elucidate phenomena that are not otherwise accessible, and are a means for careful reproducible measurements that can sometimes discover unexpected new physics.

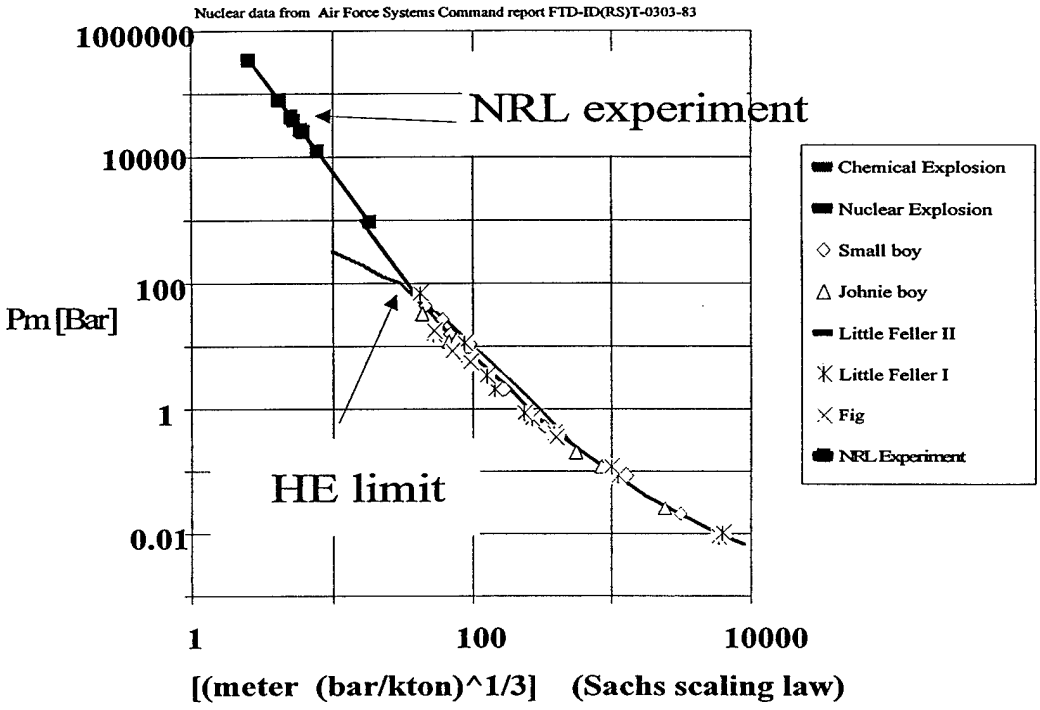

Figure 2

Laser-created shock overpressures compared to ideal overpressures and overpressures created by chemical explosives. Shocks created by nuclear explosions follow the ideal curve. The horizontal axis is the distance from the explosion point scaled with (ambient pressure/explosion yield)$^{1/3}$

Unstable Shock in a Uniform Ambient

Approximately spherical shocks were produced by heating 6-micron thick polystyrene foils, placed in an atmosphere of either 5-torr of nitrogen or xenon gas, with a 3-TW/cm^2 laser pulse. Shock evolution was followed with a fast, 120-psec to 5-nsec shutter duration, 4-frame camera and with dark-field shadowgraphy having less than 1 nsec resolution. Also, optical emission from the ambient atmosphere before and after the passage of the shock was imaged with a spectrometer coupled to a streak camera. We found that shocks in nitrogen, as expected, were always stable and smooth -- in sharp contrast to shocks launched in xenon, which were wrinkled like the example in Figure 3. The Fourier transform of the outer edge of the shock front, presented as A(k)/R vs. $\log_{10}$(kR), is shown in Figure 4. Here, A(k) is the full amplitude of the mode with wave number k and R is the average radius of the shock boundary. We see that until 18 ns the ripples do not grow. By 25ns the surface of the shock becomes significantly rippled and A(k)/R increases as a power of time. Significantly, 25ns is the time at which a Taylor-Brode-Sedov shock with its classical time$^{2/5}$ dependence has formed. (We know this from measurements of the average shock position vs. time.) The growth continues until 300ns, at which time the shock becomes smoother again and propagates as a slightly structured but a basically stable entity.

A power law of the form A(k)/R $\propto$ time$^{S(kR)}$ was fitted to the data during the period of growth, with the results shown in Figure 5. We find clear growth for modes satisfying $0.7 < \log_{10}(kR) < 2$. Maximum growth occurs at $\log_{10}(kR) = 1$, where S=1.6 and minimum growth occurs at $\log_{10}(kR) = 2$-3 with S = 0.3. The power-law fit is good (correlation >0.7) for $\log_{10}(kR) < 1.5$ but worse for larger values where the data is more noisy. The lowest growth with S = 0.3 may be a floor set by the noise in the data.

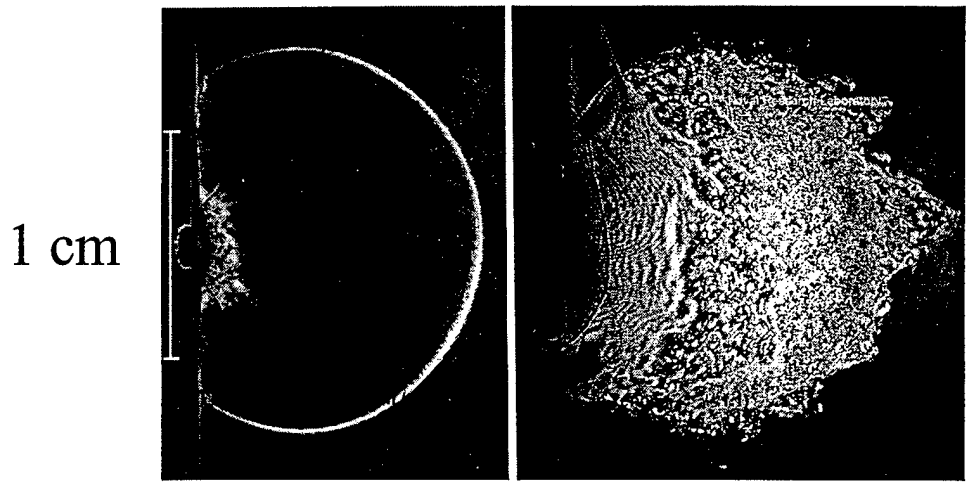

Figure 3

Stable shock in nitrogen gas and an unstable shock in xenon gas imaged with dark-field shadowgraphy.

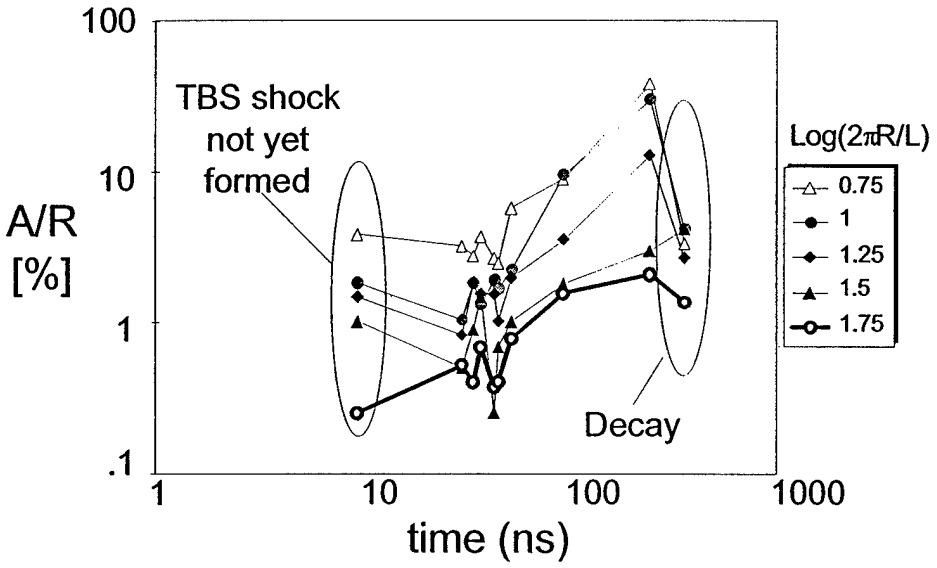

Figure 4

Growth in time for different values of $\log_{10}(kR)$.

What is so special about xenon that it causes shocks to become unstable? We believe the instability is related to the low adiabatic index γ of heated xenon. The adiabatic indices of nitrogen and xenon were determined by observing the propagation of shocks in each gas, fitting the result to the Taylor-Brode-Sedov [10] relation

$$R \cong \zeta(E/\rho_0)^{1/5}\, t^{2/5}, \quad \text{with} \quad \zeta = \left[\frac{75(\gamma-1)(\gamma+1)^2}{16\pi(3\gamma-1)}\right]^{1/5}, \tag{1}$$

where E is the explosion energy, ρ_0 is the ambient-gas density, t the time of observation, and solving for γ. This procedure yields a γ of 1.3± 0.1 for nitrogen and 1.06± 0.02 for xenon. The adiabatic index of xenon is lower than that of nitrogen because xenon gas, heated by emissions from the laser-heated target, radiates much more effectively than nitrogen, increasing the degrees of freedom within the gas and thereby decreasing γ. The enhanced radiation from xenon gas was confirmed experimentally with the spectroscopic diagnostic.

The power-law growth rate of the shock perturbations in this experiment as well as the fact that the perturbation grew only when γ was low and when a Taylor-Brode-Sedov shock developed agree reasonably well with a linear theory by Vishniak and Ryu [11] who studied the stability of shock waves in the context of supernovae. They argued that an imbalance between the thermal pressure behind a Taylor-Brode-Sedov shock and the ram pressure (ambient density times shock velocity squared) in front of the shock would redistribute mass within the shock-shell leading to oscillations that grow when $\gamma < 1.2$. Their linear theory was extended to the nonlinear regime by Mac Low and Norman [9] who calculated the stabilization we observed at times > 300ns and discussed the relevance of the instability to supernovae explosions, star formation, and to the formation of globular clusters.

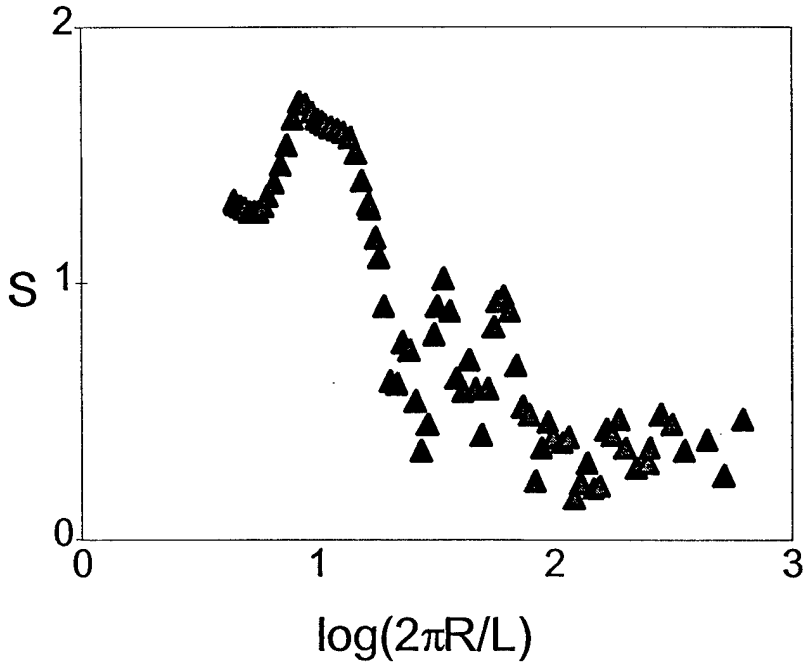

Figure 5

Growth exponent S(kR)

Decursor Shock

It is known that a shock colliding with a planar surface sets up a reflection that propagates back into the ambient gas heated by the passage of the incident front. The interacting incident and reflected shocks form Mach stems and triple points.[12] More complex structures can form if the reflecting surface is shaped, or if the sound speed near the surface varies. If the sound speed near the reflecting surface is slower than in the rest of the ambient gas a part of the shock will lag behind the rest forming a structure called a decursor.

A decursor was first observed in our experiment and later confirmed in an underground nuclear explosion test called Diamond Fortune.[13] A likely explanation of why our experiment forms decursors is that the material ablated or vaporized from the reflecting plane forms a layer with increased density and/or effective mass, and a lower sound speed. The source of energy for this ablation is radiation from the laser-heated plasma and/or the shock. Radiant energy from plastic and aluminum targets which are heated to 800 eV constitutes approximately 5% and 25% of the incident laser energy respectively.[14]

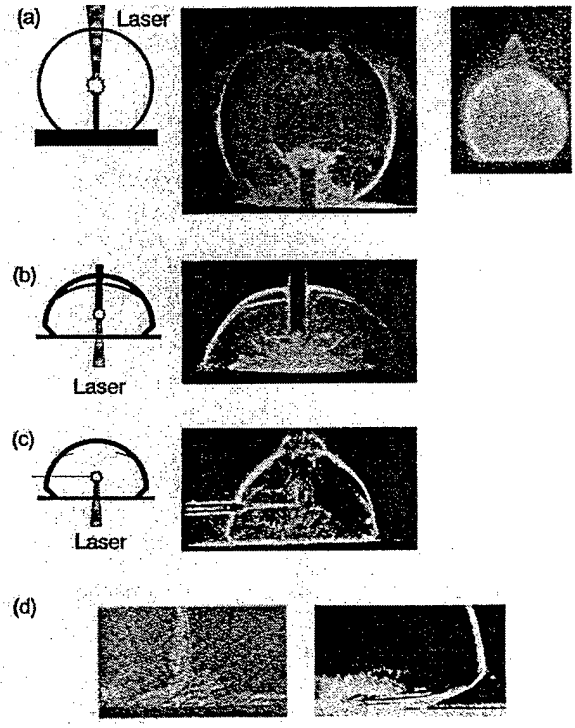

Figure 6

Structuring of shocks near reflecting, aluminum surfaces as seen with dark-field shadowgraphs and visible emission photographs. The shocks originate about 6mm above the surface and propagate in 5 torr of nitrogen. a) Spherical shock originating at the tip of an aluminum rod as observed 185ns after explosion. The laser energy was 210 joules. b) Mach stem, triple point, and decursor formation in a shock originating at the tip of an aluminum rod. The laser energy was 100 joules and the observation was at 302ns. c) A shock from a plastic target shows Mach stems, triple points, and a strong decursor 357ns after explosion. Laser energy was 103 joules. d) Close-ups of different decursor shapes observed in this experiment.

Different shock-surface configurations are shown in Figure 6. Figure 6a shows a shock soon (185ns) after it hit an aluminum plane placed 6mm below the laser's point-of-focus. The shock shows up as a bright circle surrounding the focus. Above the aluminum plane are seen diffuse, bright features that rise to the point-of-focus immediately

below the explosion, but stay closer to the plane as the lateral distance from the explosion increases. Similar features, which surround the point-of-focus itself are seen in both the dark-field and emission photographs. These diffuse features, which do not exhibit any sharp characteristics associated with shocks, are signatures of material ejected from the target and also of material ablated or vaporized from the surface of the reflecting plane by radiation from the focus region or the shock front. The reflected part of the shock is buried within the features of the ionized gas and is, therefore, not clearly visible. A dark, circle near the top of the photograph marks the passage of the laser beam. Figure 6b, taken later at 302ns, shows well developed Mach stems and triple points. As in the previous picture, there is evidence of ionized material around the focal point and near the reflecting plane. Where the shock meets the plane we see the rounded, tucked-back features of a decursor. Much clearer and stronger decursors are seen in Figure 6c, observed at 357 ns after explosion. By this time the diffuse plasma features near the plane are no longer seen. The decursors is also straighter then the rounded decursor in the previous shot. The same photograph also shows Mach stems and triple points.

Thermal Precursor Shock

A thermal shock precursor forms when a shock wave propagating through ambient air encounters a layer of hot gas whose sound speed is higher than the sound speed in the ambient. Precursor formation begins when, as a result of the higher sound speed, the incident shock wave refracts into the hot layer creating a toe wave that accelerates ahead of the main shock. The toe wave pulls gas from behind the main shock, leading to the formation of vortical flow and an increased dynamic pressure within the hot layer which drives another shock, the reflected precursor, that joins the incident and precursor shocks at the triple. High pressure behind the reflected precursor helps to sustain the gas flow, resulting in further growth of the toe wave. Thermal precursor shocks, which were first observed in nuclear explosions as early as Trinity,[15] are thought to play a role during explosive breakup of meteorites in the atmosphere, high-velocity impact of cosmic bodies on planetary surfaces, and in the interaction of interplanetary shocks with the geomagnetic tail. [16,17] Some have even suggested harnessing artificially induced precursors to alter the trajectories of small but dangerous asteroids entering the earth's atmosphere.[18]

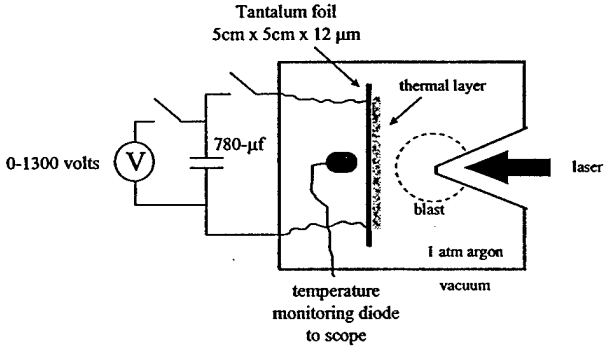

Figure 7

Setup of thermal precursor experiment.

The experiment took place inside an aluminum box of ~ 15-cm length per side (Figure 7). A hollow cone positioned with its apex protruding into the box was attached to one of the box walls. The cone's tip was cut off leaving a 1-mm diameter opening that was closed by a 2.5-μm thick layer of mylar. Inside the box was a 5 cm x 5 cm x 12 μm tantalum sheet oriented with its surface perpendicular to the cone axis and attached in series to a switched 780–μf external capacitor charged by a 1.3-kV power supply. Glass windows on the box's two opposite walls allowed viewing and access to optical diagnostics. To produce a precursor shock the box was first placed inside a larger vacuum chamber, both the box and the chamber were evacuated, and the box was back-filled with

one atmosphere of argon gas. The capacitor was then discharged through the tantalum foil, heating the foil (to as much as 3000°K) and a thin layer of argon gas above it. One millisecond later the laser was fired to produce a shock.

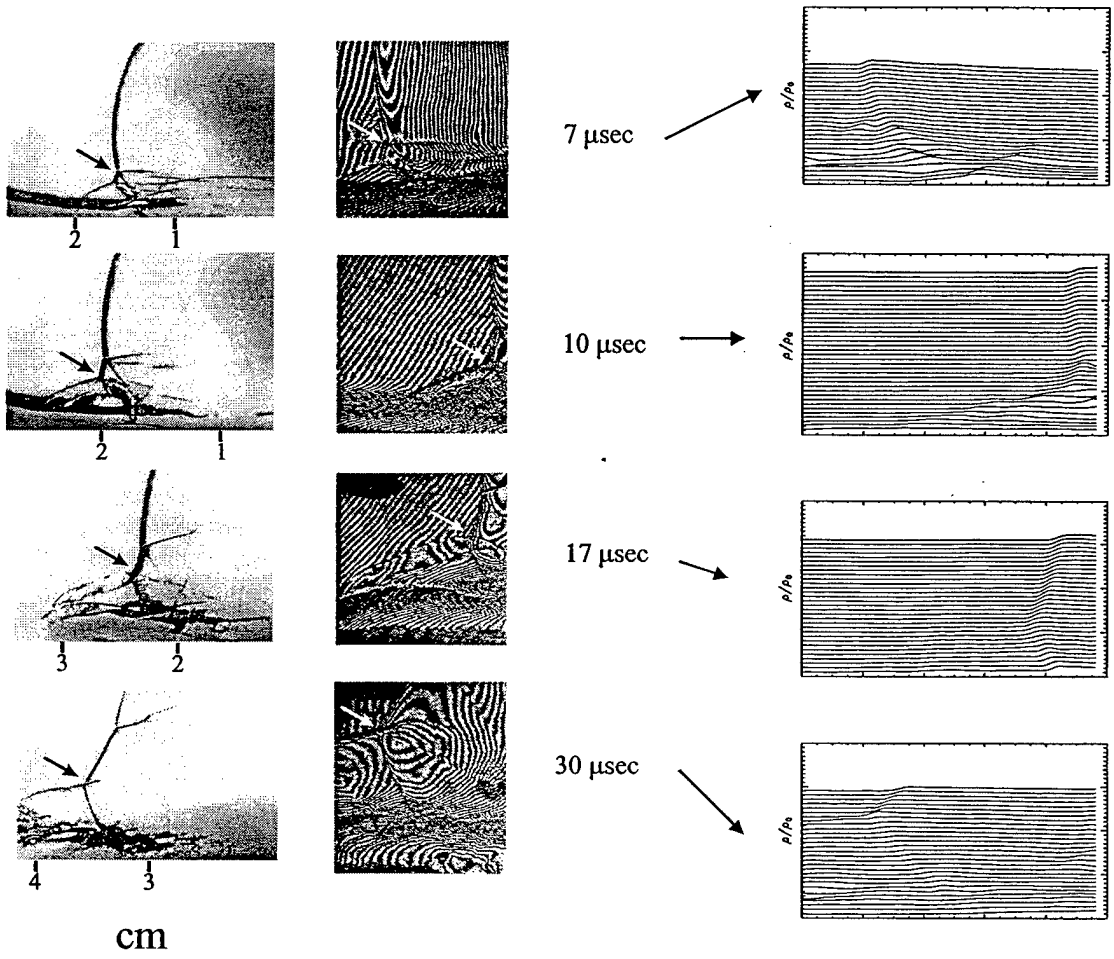

Figure 8

Precursor development. Dark-field shadowgraphs are shown on the left and interferograms in the middle. On the right are graphs of ρ/ρ_0 determined from the interferographs. . In the undisturbed region $\rho/\rho_0 = 1$. The y-axis also measures the relative density; the spacing between adjacent ρ/ρ_0 tick marks is unity.

Figure 8 shows development of the shock. The principal shock, initiated 11.5 mm above the surface, was first observed at 6.8 μsec when its radius was 17.8 mm: In the subsequent 23.6 μsec it propagated to 32.6 mm. The precursor, conversely, was 2.5 mm long at 6.8 μsec and developed to a length of 6.6 mm by 17.4 μsec. From expressions for shock pressure P and shock velocity $\dot{r}$

$$P = \frac{2}{\gamma + 1} \rho_0 \dot{r}^2 [1 - \frac{(\gamma - 1)}{2\gamma} \frac{c^2}{\dot{r}^2}] \qquad (2)$$

$$\dot{r} = \frac{2r}{5t} \tag{3}$$

where c, the sound speed in argon at room temperature, is 330 m/sec, we infer that at the first observation the pressure of the principal shock was 13-17 atmospheres, for a pre-shock γ between 5/3 and 1 respectively, and at the last observation 2-3 atmospheres. More precise Hugoniot calculations using the SESAME 5172 [19] equation-of-state table for argon yield pressures very close to those obtained from equations 2-3 with a γ of 5/3 (pre and post shock): At 6.84 μsec they give a pressure of 13.1 atm, at 21.3 μsec a pressure of 8.4 atm, and at 30.4 μsec a pressure of 2.0 atm. The density profiles inside and outside the shocks are determined from interferometry analyzed using the inverse Abel transform method.[20] The results of the analysis are shown in Figure 8.

The experiment was modeled with the second-order hydrodynamics code SHARC running in 2D axisymmetric geometry. There are no free parameters in the code and the models are quite general so that the coding used to simulate our laboratory experiment was identical to that used in simulations precursor phenomena initiated by large-scale explosions. The simulation was initiated with by heating a 1 mm-radius sphere of ambient density argon (represented by the LANL SESAME equation of state #5172) to produce a shock that was identical to the initial free-field shock that was measured. The density profile of the thermal layer was taken from the measurements. For most of the calculations the surface of the tantalum foil was assumed to be smooth. In a few cases the surface roughness was increased to 65μm, but that made virtually no difference.

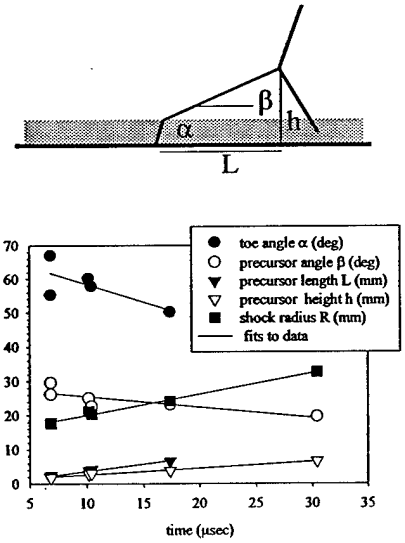

Time (μsec)	Height (mm)	Length (mm)	Angle β (deg.)
6.84	2.0	1.6	36.0
10.4	2.8	3.9	25.4
17.4	4.6	7.6	24.9
30.4	7.4	13.3	21.0

Figure 9

Measured and calculated precursor parameters agree to within ~ 10%.

Figure 9 compares calculated and measured parameters of the precursor shock. The simulation and experiment agree within ~10% if the lower-bound of the measured temperature in the thermal layer is used: Generally, the calculated precursor height and length are slightly larger than measured especially at the later times. Table I compares the simulated and measured densities behind the shock fronts. The good agreement between experiment

and simulations, evident from the figures and tables, extends the regime of validity of the computational model, previously used to simulate large shock phenomenology, into a new regime of size, time and energy scales. Furthermore, in a calculation of a replica of the experiment scaled up using Energy$^{1/3}$ scaling to 1 x 10^{12} in energy and 1 x 10^{4} in length and time the code produced results virtually identical with scaled-up results of the experiments.

Time (μsec)	Location	P_s/P_0 calculated	ρ_s/ρ_0 calculated	ρ_s/ρ_0 measured
6.84	Free field	13.1	3.1	2.7
10.4	Free field	7.33	2.7	2.5
17.4	Mach stem	9.7	2.9	2.7
30.4	Mach stem	5.33	2.6	2.3

Table 1

Simulated and measured Hugoniot states agree to within ~10%.

Summary

This paper summarizes three precision-scale experiments utilizing laser-driven shocks. One example shows measurements of a shock instability performed on centimeter spatial scales and microsecond temporal scales that are applicable to phenomena occurring on light-year spatial scales and many-years time scales. Two examples showed measurements of shock phenomena that have been reproduced on larger scale or successfully modeled with an unmodified code previously validated in large-scale tests. We feel that the prospects for meaningful precision-scale laboratory simulations to study the properties of hydrodynamic phenomena occurring at large scales are very good.

This work was supported by the Defense Special Weapons Agency.

References

[1] B.H. Ripin, A.W. Ali, H. Griem, J. Grun, S. Kacenjar, C.K. Manka, E.A. McLean A.N. Mostovych, S.P. Obenschain, J.A. Stamper, in *Laser Interaction and Related Plasma Phenomena*, Vol. 7, pg. 857, eds. H. Hora and G.H. Miley editors, (Plenum Press, NY, 1986).

[2] P.G. Sachs, " The Dependence of Blast on Ambient Pressure and Temperature", Aberdeen Proving Ground, Maryland, BRL Report No. 466 (1944).

[3] C. Manka, J. Grun, A. Fisher, R. Burris, Bull. Am. Phys. Soc. 40,11, pg.1852 (1995)

[4] A.C. Buckingham and Jacob Grun, Proc. 4th International Workshop on the Physics of Compressible Turbulent Mixing, eds. P. Linden, D. Youngs, Cambridge Univ. Press (1993); A.C. Buckingham and J. Grun Proceedings of the 4th International Workshop on the Physics of Compressible Turbulent Mixing at Cambridge University, UK 29 March-1 April 1993.

[5] R.C. Elton, D.M. Billings, C.K. Manka, H.R. Griem, J. Grun, B.H. Ripin, and J. Resnick, Physical Review E 49, pg. 1512 (1994).

[6] B.H. Ripin, A.W. Ali, H. Griem, J. Grun, S. Kacenjar, C.K. Manka, E.A. McLean A.N. Mostovych, S.P. Obenschain, J.A. Stamper, in Laser Interaction and Related Plasma Phenomena, Vol. 7, pg. 857, edited by H. Hora and G. H. Miley (Plenum Publishing, 1986); B.H. Ripin, E.A. McLean, C.K. Manka, C. Pawley, J.A. Stamper, T.A. Peyser, A.N. Mostovych, J. Grun, A. B. Hassam, and J. Huba, Phys. Rev. Let., 59, 2299 (1987); C.K. Manka, T.A. Peyser, B.H. Ripin, J.A. Stamper, J. Grun, J. Crawford, A. Hassam, J.D. Huba, Laser Interaction with Matter, pg 401, Eds: G. Velarde,E. Minguez, J. Perlado, (World Scientific Pub. Co., Sigapore 1989); B.H. Ripin, J. Grun, C.K. Manka, J.A. Stamper, E.A. McLean, J. Resnick, R. Burris, J. Crawford, J.D. Huba, and G. Ganguli, Conference Proceedings No. 485 of the AGARD Conference on Ionospheric Modification and its Potential to Enhance or Degrade the Performance of Military Systems, pg. 32-1 (1992); B.H. Ripin, J.D. Huba, E.A. McLean, C.K. Manka, T. Peyser, H.R. Burris, and J. Grun, Phys. Fluids B 5 (10), pg. 3491 (1993); B.H. Ripin, J. Grun, C.K. Manka, J.A. Stamper, E.A. McLEan, J. Resnick, R.H. Burris, J. Crawford, J.D. Huba, G. Ganguli, Proccedings of the NATO AGARD Symposium on Ionospheric Modification and Its Potential to Enhance or Degrade the Performance of Military Systems, MAY ,1990, Bergen Norway.

[7] J. Grun, J. Stamper, C.K. Manka, J. Resnick, R. Burris, and B.H. Ripin, Appl. Phys. Lett. 59 (2), pg. 246 (1991); J. Grun, C.K. Manka, B.H. Ripin, A.C. Buckingham, and I. Kohlberg in " Shock Waves at Marseille IV", R. Brun and L.Z. Dumitrescu, editors (Springer- Verlag, Berlin 1995); J. Grun, R. Burris, G. Joyce, S. Slinker, J. Huba, K. Evans, C.K. Manka, J.R. Barthel and J.W. Wiehe, Accepted by the Journal of Applied Physics (Sept. 1997); I. Kohlberg, B.H. Ripin, and J. Grun,in " Shock Waves at Marseille IV", R. Brun and L.Z. Dumitrescu, editors (Springer- Verlag, Berlin 1995).

[8] J.Grun, J. Stamper, C. Manka, J. Resnick, R. Burris, J. Crawford, Phys Rev. Lett. 66, pg. 2738 (1991).

[9] M. M. Mac Low and M.L. Norman, The Astrophysical Journal 407, pg. 207 (1993).

[10] "Physics of Shock Waves and High-Temperature Hydrodynamic Phenomena", Ya. B. Zel'dovich and Yu. P. Raizer, (Academic Press, New York, 1966).

[11] E.T. Vishniac, Astrophys. J. 274, 152 (1983); D. Ryu and E.T. Vishniac, Astrophys. J. 313, 820 (1987).

[12] "Explosive Shocks in Air", G.F. Kinney and K.J. Graham, (Springer-Verlag, New York,

[13] J.R. Barthel, J.R. Rogers, M.C. Friedman, B.F. Mason, K.D. Schneider, and J.W. Wiehe, Defense Special Weapons Agency Report DSWA-TR-97-18, (1997) (CFRD); J.R. Barthel, K.D. Schneider, J.W. Wiehe, and M.C. Friedman, Defense Special Weapons Agency Report DNA- TR-94-67, (1994) (CFRD); H. Troy, T. Pierce, S. Rogers, J. Barthel, S. Peyton, Defense Special Weapons Agency Report DSWA-TR-95-127 (1997) (CFRD); C. Petersen and P. Coleman, Defense Nuclear Agency Project Officers Report POR-7461 (1994) (UNCLASSIFIED).

[14] A few representative references: M. Galanti and N.J. Peacock, J. Phys. B: Atom. Molec. Phys., Vol 8, No. 14 pg 2427 (1975); D. Duston and J. Davis, Physical Rev. A, Vol 23, Num. 5, pg 2602 (1981);

B.K. Sinha, J. Appl. Phys. Vol 52, pg 5010 (1981); U. Feldman, et al., The Astrophysical Journal, Vol 192 Pg. 213 (1974); P.G. Burkhalter, et al., Phys. Fluids, Vol 26, pg 3650 (1983).

15 *The effects of Nuclear Weapons*, Eds. S. Glasstone and P.J. Dolan (United States Department of Defense and the Energy Research and Development Administration, Washington DC, 1977).

16 V.I. Artem'ev, V.I. Bergel'son, S.A. Medvedyuk, I.V. Nemchinov, T.I. Orlova, V.A. Rybakov, and V.M. Khazins, Fluid Dynamics 32, pg. 121 (1996); references therein.

17 P.E. Alexandrov, Journal of Engineering Physics and Thermophysics 64, pg. 444 (1993).

18 I.V. Nemchinov, V.I. Artem'ev, V.I. Bergelson, V.M. Khazins, T.I. Orlova, and V.A. Rybakov, Shock Waves 4, pg. 35 (1994).

19 *T-4 Handbook of Material Properties Data Base, Vol. 1c: Equation of State*, K.S. Holian, ed., Los Alamos National Laboratory report LA-10160-MS UC-34 (1984).

20 *Holographic Interferometry*, C.M. Vest, (Wiley, New York, 1979).